

Distinct Fermi-Momentum Dependent Energy Gaps in Deeply Underdoped Bi2212

Kiyohisa Tanaka,^{1,2} W.S. Lee,¹ D.H. Lu,¹ A. Fujimori,³
 T. Fujii,⁴ Risdiana,⁵ I. Terasaki,⁵
 D.J. Scalapino,⁶ T.P. Devereaux,^{7,8} Z. Hussain,² and Z.-X. Shen,^{1*}

¹Department of Physics, Applied Physics, and Stanford Synchrotron Radiation Laboratory,
 Stanford University, Stanford, CA 94305, USA

²Advanced Light Source, Lawrence Berkeley National Lab, Berkeley, CA 94720, USA

³Department of Physics and Department of Complexity Science and Engineering,
 University of Tokyo, Kashiwa, Chiba 277-8561, Japan

⁴Cryogenic Center, University of Tokyo, Bunkyo-ku, Tokyo 113-0032, Japan

⁵Department of Applied Physics, Waseda University, Tokyo 169-8555, Japan

⁶Department of Physics, University of California, Santa Barbara, CA 93106-9530, USA

⁷Department of Physics, University of Waterloo, Ontario N2L3G1, Canada

⁸Pacific Institute for Theoretical Physics, University of British Columbia,
 Vancouver, British Columbia, V6T 1Z1, Canada

*To whom correspondence should be addressed; E-mail: zxshen@stanford.edu.

We use angle-resolved photoemission spectroscopy applied to deeply underdoped cuprate superconductors $\text{Bi}_2\text{Sr}_2(\text{Ca},\text{Y})\text{Cu}_2\text{O}_8$ (Bi2212) to reveal the presence of two distinct energy gaps exhibiting different doping dependence. One gap, associated with the antinodal region where no coherent peak is observed, increases with underdoping - a behavior known for more than a decade and considered as the general gap behavior in the underdoped regime. The other gap,

associated with the near nodal regime where a coherent peak in the spectrum can be observed, does not increase with less doping - a behavior not observed in the single particle spectra before. We propose a two-gap scenario in momentum space that is consistent with other experiments and may contain important information on the mechanism of high- T_c superconductivity.

The pseudogap phase of underdoped cuprates has proven to be an important region for discoveries and surprises in the field of high-transition temperature (T_c) superconductors (1). Early angle-resolved photoemission (ARPES) (2) and electron tunneling experiments from lightly underdoped samples (3) suggested that the pseudogap has similar characteristics to the superconducting gap below T_c , consistent with the idea that the pseudogap is a precursor to the $d_{x^2-y^2}$ superconducting state but lacks pair phase coherence. In this scenario, below T_c where the phase coherence of pairs is established, the pseudogap smoothly evolves into the superconducting gap. There is only one energy scale in the system and is associated with the magnitude of the gap at the antinode. This antinodal gap was found via ARPES (4), thermal conductivity (5), and tunneling measurements (6) to increase as the doping was reduced from optimum. However, the energy gap obtained by Andreev reflection (7), penetration depth (8), and recent Raman experiments (9, 10) of cuprates exhibits the opposite trend with doping suggesting a rather different scenario from the one-gap picture.

We present ARPES data for deeply underdoped $\text{Bi}_2\text{Sr}_2(\text{Ca},\text{Y})\text{Cu}_2\text{O}_8$ (Bi2212) crystals with T_c values of 50 K, 40 K, and 30 K, finding evidence for the existence of two distinct energy gaps in the single-particle spectral function (See “Supporting Online Materials” for details about materials and the ARPES measurements setup). One gap manifests itself as a spectral weight suppression near the Brillouin zone boundary (antinodal region); this

antinodal gap becomes larger with decreased doping, consistent with previous ARPES studies (4). The other gap is resolved near the diagonal of the zone (nodal region) where a quasi-particle peak can be observed. We find that the gap size of this near nodal gap determined by empirical methods does not increase by decreasing doping level. We attribute our result as evidence for two distinct Fermi momentum dependent energy gaps, with the gap near the nodal region corresponding to the superconducting gap and the gap near the antinodal region to the pseudogap state.

In Fig. 1, we show energy distribution curves (EDCs) along the Fermi surface (FS) for the $T_c = 50$ K, 40 K, and 30 K samples. Compared to previous ARPES studies on underdoped Bi2212 with a similar doping level (11), our new data have a much improved quality; even for the most underdoped sample ($T_c = 30$ K), a clear quasi-particle (or coherence) peak can still be observed near the nodal region (Fig. 1B), which has not been seen previously in Bi2212 for such a low doping. This improvement makes possible a more quantitative data analysis. We first note that the lineshape of the spectra shows a marked change along the FS. The sharp coherence peak gradually loses spectral weight when moving from the nodal region toward the antinodal region. In the antinodal region, the peak disappears and only a broad hump in the spectrum located far away from the Fermi level (E_F) can be observed for the $T_c = 30$ K and 40 K samples. This behavior is consistent with previous studies of other underdoped cuprates such as $\text{La}_{2-x}\text{Sr}_x\text{CuO}_4$ (LSCO) and $\text{Ca}_{2-x}\text{Na}_x\text{CuO}_2\text{Cl}_2$ (Na-CCOC) (12, 13). Here, we operationally define the Fermi arc as the region where one can see a peak in the superconducting state EDCs. Clearly, as demonstrated in Figs. 1B-G and the inset of Fig. 1H, the length of the Fermi arc decreases as the doping level of the samples decreases.

In Fig. 1H, we plot the leading-edge gap, defined as the energy difference between the mid-point of the spectral leading edge and that of the nodal spectrum within the Fermi arc

region. We find that the leading-edge gap is smaller for the lower T_c samples suggesting that the energy gap associated with this Fermi arc region decreases with decreased doping. This doping dependence can be directly observed in the raw spectrum. The EDCs in the intermediate region (Fig. 1E) show that both the coherence peak position and the leading-edge gap of the $T_c = 50$ K sample is larger than the $T_c = 40$ K and 30 K samples. Similar observation can also be deduced from Fig. 1, C and D, which are all still within the Fermi arc region. This gap-reduction trend within the Fermi arc region is opposite to the doping dependence of the energy gap in the antinodal region reported in previous ARPES studies (4), and is in conflict with the doping dependence of the energy gap inferred from thermal conductivity (5) and tunneling measurements (6).

In the antinodal region, the spectrum is characterized by a suppression of the spectral weight over a region which one associates with a pseudogap. To illustrate the difference in the doping dependence of the pseudogap and the energy gap associated with the Fermi arc, we have plot symmetrized EDCs (14) for the three samples for an intermediate Fermi arc k-point (point 8), and an antinodal k-point (point 16) (Fig. 2A, B). As indicated by the shaded areas, it is clear that the EDCs of point 16 show a larger gap with more underdoping while the EDCs of point 8 exhibit the opposite trend with doping. The inset in Fig. 2B shows that there is essentially no change in the EDC of the $T_c = 30$ K sample between the superconducting ($T = 10$ K, blue line) and the normal state ($T = 50$ K, red line) in the antinodal region. It also suggests that the broadening of the peak with temperature does not shift the leading-edge position downwards in these deeply underdoped samples. For a more comprehensive view of the trend, the peak positions of EDCs relative to the node at various locations near the intermediate region (point 6, 8, and 10) and the antinodal region (point 16) are plotted (Fig. 2C). Clearly, the doping dependence of the energy gap along the Fermi arc and the antinodal region are different. This behavior suggests

that the energy gaps associated with the Fermi arc region and antinodal region represent two distinct energy gaps arising from different mechanisms. The antinodal gap appears to be related to the pseudogap and not related to superconductivity; whereas, the nodal gap more likely represents the “real” superconducting gap because of the existence of a coherence peak in the spectrum. The distinction between the two gaps becomes smaller and harder to observe towards optimum doping (1, 2, 3, 4). While an earlier experiment near optimal doping has seen this same trend, the result was attributed to an anharmonic term in the d -wave gap (15). Uncovering the distinct spectral lineshape in these deeply underdoped samples makes it possible to attribute to distinct energy gaps.

As the energy gap in the antinodal region is primarily dominated by the pseudogap, it is not straightforward to estimate the magnitude of the maximum superconducting gap Δ_0 . Here, we exploit a phenomenological method to estimate Δ_0 . The EDCs along the Fermi arc are first divided by the Fermi-Dirac (FD) function at the measurement temperature convoluted with the experimental resolution (Fig. 3A). In this way, one can track the peak position of the single-particle spectral function without the complications of FD cut-off near E_F . We then plot the peak position of these spectra with respect to the $d_{x^2-y^2}$ function ($|\cos k_x - \cos k_y|/2$), as illustrated in the inset of Fig. 3A. It can be seen that the peak positions of these FD-function divided spectra lay on a straight line for k_F values in the nodal region, suggesting that the superconducting gap around the nodal region is consistent with this $d_{x^2-y^2}$ form. We then estimate Δ_0 by extrapolating this straight line to the boundary where $|\cos k_x - \cos k_y|/2 = 1$, as shown in the inset of Fig. 3A. Using this method, we extract Δ_0 for samples with various doping levels and summarize the result in Fig. 3B. The values of Δ_0 determined in this way increases as the doping changes from $T_c = 30$ K to $T_c = 50$ K, consistent with the behavior of the peak positions shown in Fig. 2C. It reaches a maximum at a doping level of approximately

0.1 and then remains at the same size (or even slightly decreases) for doping levels up to the optimal doping level. We note that similar behavior appears in results obtained from Nernst effect measurements (16). Thus, taken at face value (17), the extrapolation of the nodal region data along with the behavior of the peak position at the points 6, 8, and 10 suggest that the gap characteristic of the nodal region has a distinct doping dependence from that of the antinodal gap. Specifically, the nodal region gap has a d -wave momentum dependence with an amplitude that remains relatively constant for a range of doping below optimal doping and then decreases as the system becomes severely underdoped.

Now, let us summarize our momentum-space picture of this two-gap scenario. Beginning with the deeply underdoped Bi2212, there is a small Fermi arc where a peak can be observed in the EDCs at the Fermi crossing points k_F . This arc, centered at the nodal k_F point, then extends out along the FS increasing in length as the doping is increased. Along this arc, we find evidence for a k -dependent gap, consistent with a superconducting $d_{x^2-y^2}$ gap with an increasing magnitude as the hole doping increases. Another pseudogap which is much larger and decreases with doping dominates the antinodal region. We believe that the smaller nodal region gap is the true superconducting gap because it exhibits a peak in the EDC. The pseudogap may arise from another mechanism such as Umklapp scattering by the antiferromagnetic correlation or competing states, such as stripes (18, 19), polaronic (20, 21) behavior, or a charge-density-wave (22, 13).

This two-gap scenario is consistent with other experiments. First, thermodynamic data suggest a distinct pseudogap and a superconducting gap (23). Second, recent Raman studies (9, 10) also suggest energy gaps extracted from B_{1g} (dominated by the antinodal region) and B_{2g} symmetry (dominated by the nodal region) have different origins with opposite doping dependence. In addition, contradictory results of the superconducting gap

deduced from different experimental tools can also be resolved within this momentum-space two-gap picture. Andreev reflection (7) and penetration depth measurement (8) clearly indicate that the superconducting gap declines with more underdoping while tunneling spectroscopy (3,6) shows the opposite trend with the doping. Such inconsistencies are difficult to explain using a one-gap scenario, but are naturally compatible with the two-gap scenario. We suggest that some measurements, such as Andreev reflection and the penetration depth, are sensitive to the superconducting condensate itself; thus, the superconducting gap near the nodal region is probed. On the contrary, STM spectrum is more sensitive to the antinodal gap because of larger phase space. Thus, the doping dependence of the energy gap obtained from STM, Andreev reflection and penetration depth is different because they are sensitive to different gaps in the FS.

This two-gap scenario has two important implications which could be very important for developing a microscopic theory of high T_c superconductivity. First, the pseudogap near the antinodal region in these deeply underdoped samples is unlikely a precursor state of the superconducting state. Second, our data suggest that the weakened superconductivity in the deeply underdoped region arises not only from the loss of phase coherence (24) due to the decrease in the superfluid density but also a weakening of the pair amplitude. In this case, a mechanism for the superconducting gap reduction could be related to the shrinkage of the coherent FS with less doping leading to a smaller phase space for pairing.

References and Notes

1. T. Timusk, B. Statt, *Rep. Prog. Phys.* **62**, 61 (1999).
2. A. G. Loeser *et al.*, *Science* **273**, 325 (1996).

3. Ch. Renner, B. Revaz, J.-Y. Genoud, K. Kadowaki, O. Fischer, *Phys. Rev. Lett.* **80**, 149 (1998).
4. J. C. Campuzano *et al.*, *Phys. Rev. Lett.* **83**, 3709 (1999).
5. M. Sutherland *et al.*, *Phys. Rev. B* **67**, 174520 (2003).
6. N. Miyakawa, P. Guptasarma, J. F. Zasadzinski, D. G. Hinks, K. E. Gray, *Phys. Rev. Lett.* **80**, 157 (1998).
7. G. Deustcher, *Nature* **397**, 410 (1999).
8. C. Panagopoulos, J. R. Cooper, T. Xiang, *Phys. Rev. B* **57**, 13422 (1998).
9. M. Opel *et al.*, *Phys. Rev. B* **61**, 9752 (2000).
10. M. Le Tacon *et al.*, *Nature Physics* **2**, 537 (2006).
11. J. M. Harris *et al.*, *Phys. Rev. B* **54**, R15665 (1996).
12. T. Yoshida *et al.*, *Phys. Rev. Lett.* **91**, 027001 (2003).
13. K.M. Shen *et al.*, *Science* **307**, 901 (2005).
14. J. Mesot *et al.*, *Phys. Rev. B* **63**, 224516 (2001).
15. J. Mesot *et al.*, *Phys. Rev. Lett.* **83**, 840 (1999).
16. Y. Wang, L. Li, N. P. Ong, *Phys. Rev. B* **73**, 024510 (2006).
17. We have fit the ARPES data using various impurity scattering (Born, unitary, forward scattering (L. Zhu, P. J. Hirschfeld, D. J. Scalapino, *Phys. Rev. B* **70**, 214503 (2004).)) models and backgrounds. However, the large number of parameters and the choice

of backgrounds make it hard to extract unique conclusions from fits. Therefore we focus directly on the data.

18. J. M. Tranquada, B. J. Sternlieb, J. D. Axe, Y. Nakamura, S. Uchida, *Nature* **375**, 561 (1995).
19. K. Yamada *et al.*, *Phys. Rev. B* **57**, 6165(1998).
20. K. M. Shen *et al.*, *Phys. Rev. Lett.* **93**, 267002 (2004).
21. A. S. Mishchenko, N. Nagaosa, *Phys. Rev. Lett.* **93**, 036402 (2004).
22. T. Hanaguri *et al.*, *Nature* **430**, 1001 (2004).
23. J. W. Loram, J. Luo, J. R. Cooper, W. Y. Liang, J. L. Tallon, *J. Phys. Chem. Solids* **62**, 59 (2001).
24. V. J. Emery, S. A. Kivelson, *Nature* **374**, 436 (1995).
25. A. Damascelli, Z. Hussain, Z.-X. Shen, Fig. 62, *Rev. Mod. Phys.* **75**, 473 (2003).
26. ARPES experiments were performed at Stanford Synchrotron Radiation Laboratory which is operated by the Department of Energy Office of Basic Energy Science under contract DE-FG03-01ER45929-A001. This work is also supported by Office of Naval Research grant N00014-01-1-0048 and NSF grant 0304981. DJS would like to acknowledge the Center for Nanophase Materials Science at Oak Ridge National Laboratory for their support.

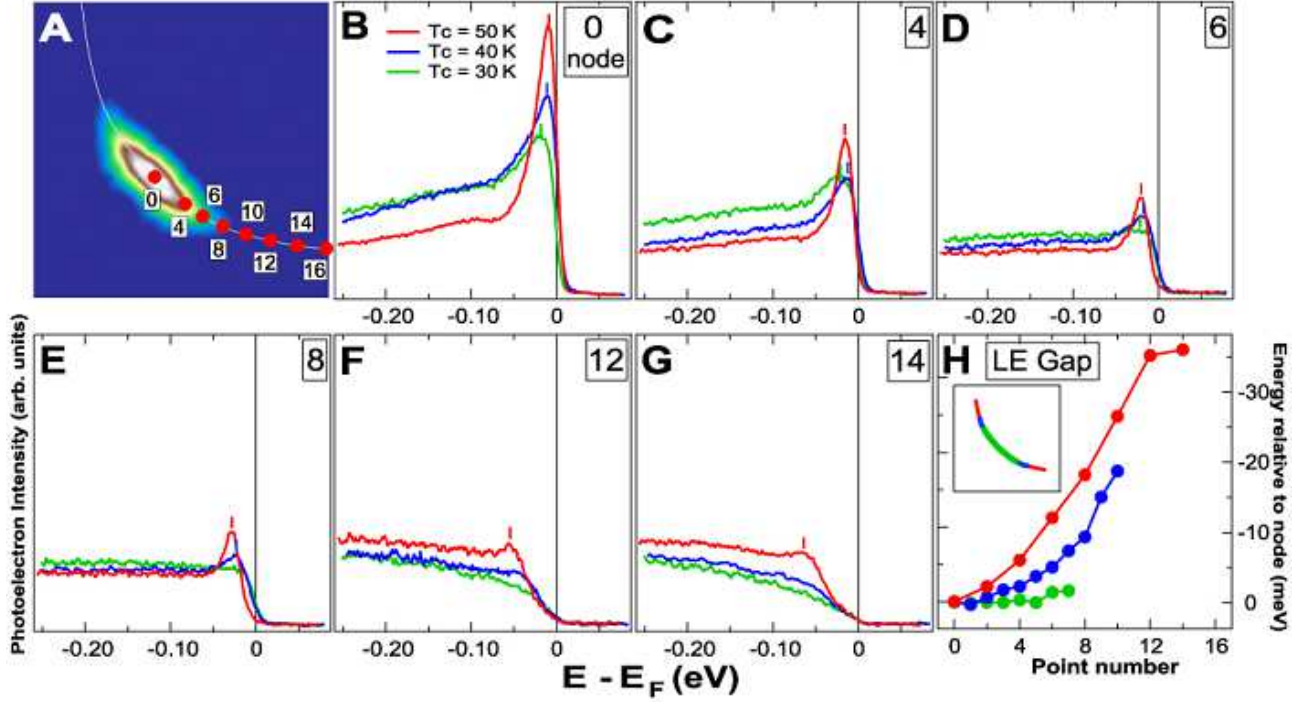


Figure 1: **Doping dependence of the ARPES spectra and leading edge position along the Fermi surface.** (A) Intensity plot of the spectral weight of the $T_c = 30$ K sample, which is integrated within ± 10 meV around the Fermi level (E_F) and symmetrized with respect to the diagonal of the zone. The intensity of diffraction replica due to supermodulation of the crystal structure has been cut off by color scale. The red dots labeled with numbers denote the Fermi crossing points k_F determined from the momentum distribution curves (MDC) at E_F . (B to G) The energy distribution curves (EDC) along the Fermi surface (FS) of the $T_c = 30, 40$, and 50 K samples. The number shown at the upper right corner corresponds to the k_F locations shown in (A). The vertical bars indicate the peak position of the EDC. The k_F region of the FS where a peak is visible in the EDCs is operationally defined as the Fermi arc. (H) Doping dependence of the leading edge position relative to that of the nodal spectrum within the Fermi arc. The inset illustrates that the Fermi arc elongates toward the antinodal region of k -space with increasing doping. The data shown in this paper were taken in the second Brillouin zone where an enhancement of the spectra is observed (See Supporting Online Materials).

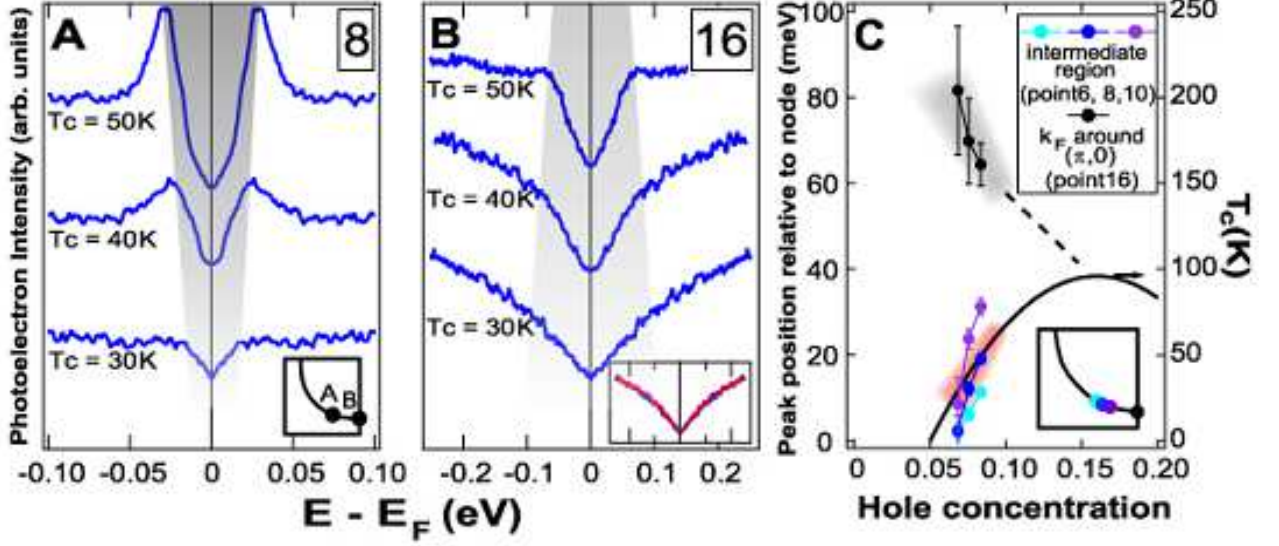


Figure 2: **Doping dependence of the symmetrized spectra at the intermediate region and the antinodal region.** The symmetrized EDCs at (A) the intermediate region of the FS (point 8 in Fig. 1A) and (B) the antinodal region (point 16). Their corresponding locations on the FS are shown in the inset of (A). The shaded area denotes the region inside the gap determined by the peak positions of the EDCs. For the antinodal spectra, the position of the hump, which is determined from the second derivative of the spectra, is used as the peak position. Inset of (B) shows temperature dependence of the spectra of the $T_c = 30\text{ K}$ sample taken at 10 K (blue line) and 50 K (red line) at the antinodal region. (C) Doping dependence of the peak position around the intermediate region (point 6, 8, and 10) and in the antinodal region (point 16) shown in the inset together with T_c . The dashed line indicates the pseudogap at the antinodal region reported by previous ARPES studies on Bi2212 system (4). Here, the hole concentration (p) was estimated by using an empirical relationship $T_c = 96(1 - 82.6(p - 0.16)^2)$.

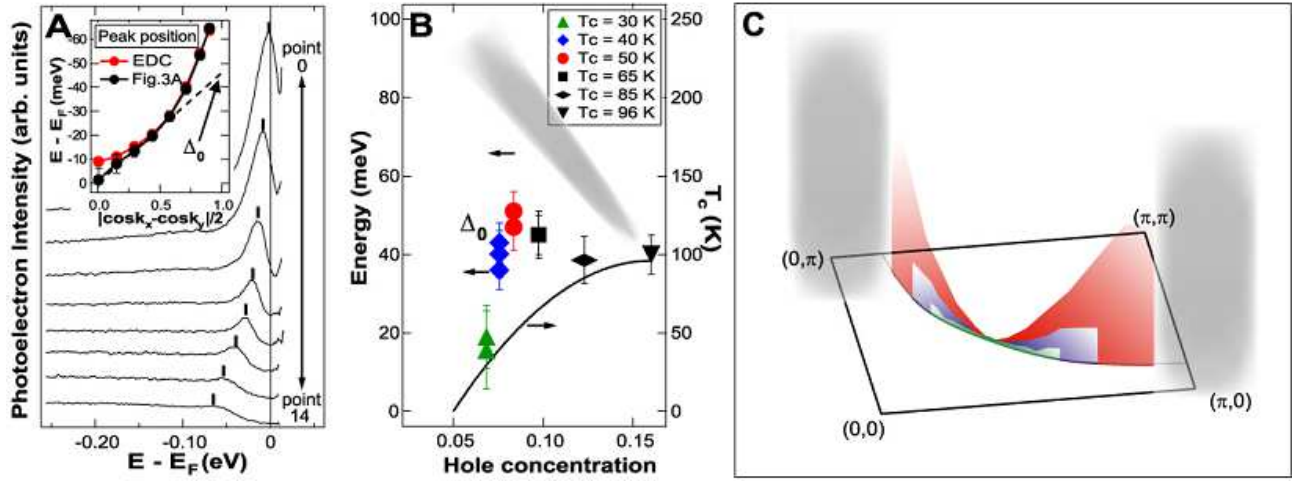


Figure 3: **Determination of Δ_0 and its doping dependence.** (A) Spectra of the $T_c = 50$ K sample along the FS which were divided by the Fermi-Dirac (FD) function convoluted with the experimental resolution. The vertical bars indicate the peak position. The inset shows a comparison of the peak position in EDCs plotted against the d -wave function ($|\cos k_x - \cos k_y|/2$) for the raw EDCs and the FD-function divided EDCs. The dashed line illustrates an extrapolation of the straight section around the nodal region of the black curve, which leads to Δ_0 at $|\cos k_x - \cos k_y|/2 = 1$. (B) Doping dependence of the Δ_0 . The gray shaded area is a guide to the eyes for the doping dependence of the energy gap at the antinodal region from data shown in Fig. 2C as well as existing published data (25). Δ_0 s for $T_c > 60$ K were taken from our ARPES studies of $\text{Bi}_2\text{Sr}_2\text{Ca}_{0.92}\text{Y}_{0.08}\text{Cu}_2\text{O}_{8+\delta}$ samples (see Supporting Online Material). (C) Doping dependence of the leading edge position in the k -space. The same color assignment as (B) is used for a easy comparison.